EurJIC European Journal of Inorganic Chemistry
ChemPubSoc Europe
FULL PAPER

DOI:10.1002/ejic.201300710

Reaction Mechanism of Water Oxidation Catalyzed by Iron Tetraamido Macrocyclic Ligand Complexes – A DFT Study

CLUSTER ISSUE

Rong-Zhen Liao,*[a] Xi-Chen Li,[a] and Per E. M. Siegbahn[a]

Keywords: Water oxidation / Reaction mechanisms / Density functional calculations / Iron

Density functional calculations are used to elucidate the reaction mechanism of water oxidation catalyzed by iron tetraamido macrocyclic ligand (TAML) complexes. The oxidation of the starting TAML–Fe^{3+}–OH_2 complex by removing three electrons and two protons leads to the formation of a key intermediate, TAML$^{\cdot}$–Fe^{5+}=O, which can undergo nucleophilic attack by either a water molecule or a nitrate ion. Both pathways involve attack on the oxo group and lead to the production of O_2. The water attack is more favoured and has a total barrier of 15.4 kcal/mol. The alternative nitrate attack pathway has a barrier of 19.5 kcal/mol. Nitrate functions as a cocatalyst by first donating an oxygen atom to the oxo group to form O_2 and a nitrite ion, which can then be re-oxidized to regenerate a nitrate ion. Three possible competing pathways result in ligand modification, namely, water and nitrate attack on the ligand, as well as ligand amide oxidation. The water attack on the ligand has a low barrier of only 10.9 kcal/mol and leads to the opening of the benzene ring, which explains the observation of fast catalyst degradation. The lack of activity or lower activity of other catalysts with different substituents is also rationalized.

Introduction

The conversion of water into molecular oxygen and hydrogen by using sunlight is a very promising process to supply a clean and renewable source of energy. The oxidation of water by the liberation of four protons and four electrons is the bottleneck in this task. The reaction is not thermodynamically favourable and is associated with a relatively large energy penalty (E_0 = 1.23 V, standard reduction potential at pH 0). In addition, an efficient catalyst with high stability and turnover number (TON) is needed to promote the O–O bond formation. Extraordinary efforts have been devoted to the development of both heterogeneous and homogeneous water oxidation catalysts (WOC),[1–7] but most are based on expensive heavy transition metals such as ruthenium[8–12] and iridium.[13–16] Therefore, it is of high interest to develop a WOC based on abundant and inexpensive first-row transition metals.[17–20] Recently, Ellis et al. synthesized five Fe^{3+} complexes based on tetraamido macrocyclic ligands (Fe^{3+}–TAMLs, Scheme 1); four of them (WOC_B–WOC_E) catalyze water oxidation in the presence of excess ceric ammonium nitrate (CAN) at pH 0.7.[21] WOC_E gave the highest activity and showed a turnover frequency larger than 1.3 s^{-1}, whereas only a small activity was observed for WOC_A. However, for WOC_E, a rapid release of O_2 could only be observed in the first 20 s, which suggests a quite fast catalyst degradation. Kinetic studies also suggest that the formation of O_2 catalyzed by WOC_E is first order and, therefore, exclude the possibility of a cooperative metal–oxo coupling mechanism, which has been found for mononuclear Ru-based catalysts.[22,23]

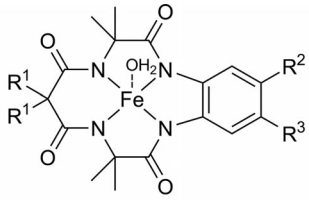

WOC_A:	$R^1 = CH_3$	$R^2 = R^3 = H$
WOC_B:	$R^1 = (CH_2)_2$	$R^2 = R^3 = H$
WOC_C:	$R^1 = F$	$R^2 = R^3 = H$
WOC_D:	$R^1 = F$	$R^2 = H$, $R^3 = NO_2$
WOC_E:	$R^1 = F$	$R^2 = R^3 = Cl$

Scheme 1. Five Fe^{3+}–TAMLs used for water oxidation.[21]

Recently, Cramer and co-workers performed density functional and multireference second-order perturbation calculations to understand the reaction mechanism of water oxidation enabled by the WOC_E catalyst.[24] They suggested that the reaction starts from two sequential proton-coupled electron transfer (PCET) steps from the TAML–Fe^{3+}–OH_2 complex to form a TAML–Fe^{5+}=O species, followed by a one-electron oxidation of the ligand to generate a

[a] Department of Organic Chemistry, Arrhenius Laboratory, Stockholm University,
Svante Arrhenius väg 16 C, 10691 Stockholm, Sweden
E-mail: rongzhen@organ.su.se
www.organ.su.se

Supporting information for this article is available on the WWW under http://dx.doi.org/10.1002/ejic.201300710.

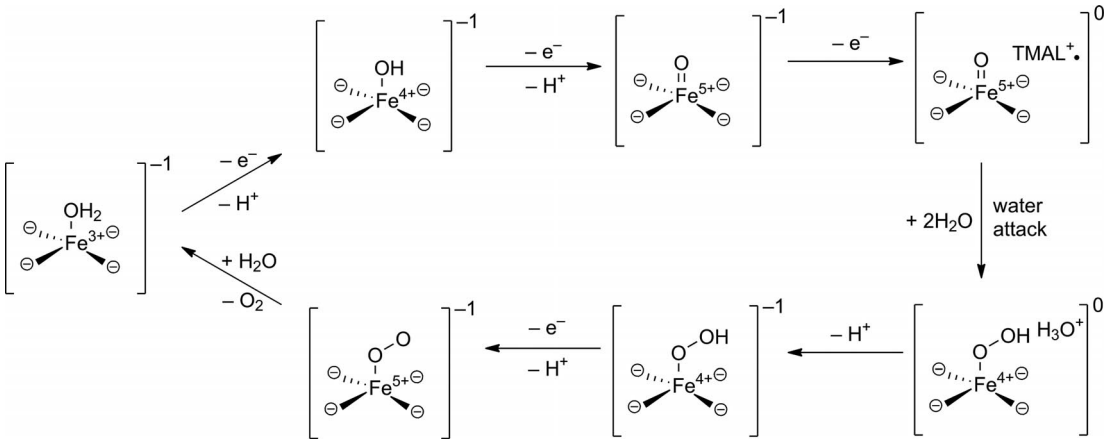

Scheme 2. Reaction mechanism proposed on the basis of previous calculations.[24]

TAML^{+}•–Fe^{5+}=O intermediate (Scheme 2). Therefore, the key oxidizing species is formally Fe^{6+}, but this high-valent oxidation state is delocalized over two redox-active centres, namely, the metal centre and the TAML ligand. A water molecule then performs a nucleophilic attack on the oxo group facilitated by a microsolvation shell of water molecules. This type of water attack mechanism has also been suggested for a number of mononuclear Co-, Ru-, and Ir-based catalysts.[25–31] This step was calculated to be rate-limiting with a total barrier of ca. 30 kcal/mol. This is much too high compared with the experimental rate constant (1.3 s^{-1}) at room temperature, which can be converted to a barrier of 17.3 kcal/mol by using classical transition-state theory. Once the O–O bond is formed, a proton can easily be released into solution to form a TAML–Fe^{4+}–OOH intermediate. Subsequently, proton-coupled electron transfer occurs, followed by O_2 release and water binding, which regenerates the TAML–Fe^{3+}–OH$_2$ species. As a technical note, the computed barrier was very sensitive to the density functional used; for example, B3LYP gives a barrier of 14.6 kcal/mol.[24]

In this paper, we revisit the reaction mechanism of this catalytic reaction by density functional calculations. An alternative mechanism involving a nitrate cocatalyst is proposed. A full energy diagram for the whole catalytic cycle is constructed, similarly to our previous studies on photosystem II and two Ru-based catalysts.[32–38] Possible competing catalyst degradation pathways, which have not been considered before, have also been explored. The lower activity and lack of activity of other complexes with different ligand substituents are rationalized by analyzing the total barriers. The secondary pathways proposed should stimulate further experimental studies to obtain more stable catalysts and to verify whether nitrate ions are involved in the water oxidation for this catalyst.

Results and Discussion

Quantum chemical calculations have been performed to elucidate the reaction mechanism of O_2 formation and the fast deactivation of WOC$_E$. Two types of mechanism, involving water and nitrate attack, will be presented and discussed for the water oxidation. Three types of competing pathways that could lead to ligand modification and catalyst deactivation will be shown. Furthermore, the lack of activity of WOC$_A$ and the relatively lower activity of WOC$_B$–WOC$_D$ will be rationalized. Finally, the computed energy profiles derived from the two different functionals B3LYP*-2D and M06L will be compared.

A. O_2 Formation by Direct Water Attack

As mentioned in the Introduction, Cramer and coworkers have suggested all intermediates and transition states for the O_2 formation by a direct water attack on the high-valent iron–oxo group.[24] In the present study, we construct the full energy diagram by using the experimental driving force, which was not done before. This will be helpful for the understanding of the rate-limiting step and the total barrier.

The resting state is a pentacoordinate ferric complex (labelled as **1**, or Fe^{3+}–OH$_2$, Figure 1) with a water molecule bound to the metal. The complex has a quartet ground state, and the sextet and doublet are 14.0 and 30.9 kcal/mol higher in energy, respectively. The first oxidation step is a one-electron oxidation to form the triplet species Fe^{4+}–OH$_2$ (**2**). This step is calculated to be exothermic by 15.1 kcal/mol (Figure 2), and, thus, the redox potential for the **2/1** pair is 1.07 V (Table 1). From **2**, a PCET oxidation takes place to form a doublet TAML•–Fe^{4+}–OH complex (**4**), which is best described as an intermediate-spin Fe^{4+} (S_{Fe} = 1) centre antiferromagnetically coupled to the ligand radical cation (S = 1/2). The quartet and sextet states are 1.6 and 19.4 kcal/mol higher in energy, respectively. Thus, during the oxidation, one electron is released from the ligand, rather than from the metal centre. The redox potential for this step is calculated to be 1.75 V. Subsequently, another PCET oxidation of **4** (redox potential 1.75 V) leads to the formation of TAML•–Fe^{5+}=O (**6**), which is the proposed oxidant for the following O–O bond formation. The ground

state of **6** is a triplet at the B3LYP*-2D level and has a low-spin iron centre (S_{Fe} = 1/2) that interacts with the TAML ligand radical cation (S = 1/2) in a ferromagnetic fashion. The broken-symmetry singlet state with the two radicals antiferromagnetically coupled is +3.0 kcal/mol higher in energy than the triplet state. In contrast to B3LYP*-2D, the

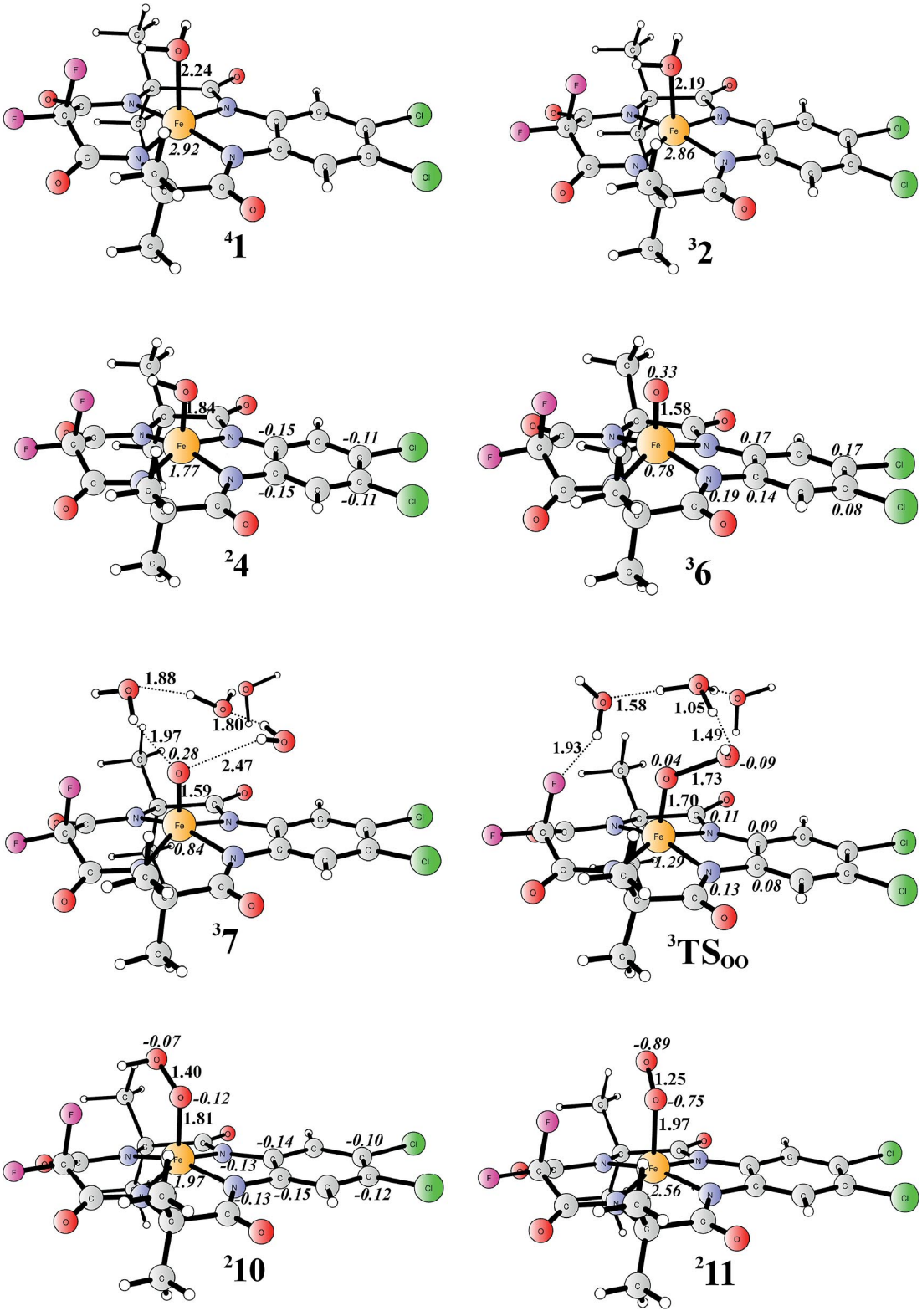

Figure 1. Selected optimized structures along the reaction pathway of direct water attack. Distances are given in angstroms. Spin densities for Fe and other important atoms are indicated in italics. For all structures, the spin state with the lowest energy is shown. Superscripts indicate the multiplicity of the structure.

M06L functional favours the singlet by 0.4 kcal/mol. Previous CASPT2 calculations showed that the singlet–triplet gap is 3.3 kcal/mol.[24] However, this gap might be overestimated as entropy corrections could favour the triplet by 1–2 kcal/mol. This is quite similar to compound I in P450 enzymes, in which the porphyrin radical cation can interact with the iron centre in both an antiferromagnetic and a ferromagnetic fashion. The electronic structure of ^{5}**6**, equivalent to TAML·–Fe^{4+}–O· and 8.3 kcal/mol higher in energy than the triplet, is best described as an intermediate-spin iron centre (S_{Fe} = 1) ferromagnetically coupled to the oxyl radical (S = 1/2) and to the TAML ligand radical cation (S = 1/2).

In the previous study it was shown that **6** is the active species for O–O bond formation by water attack.[24] The authors suggested that a proper description of this process requires four water molecules. The main reason for the addition of more water molecules is that a proton is released into solution during the attack, and two additional water molecules are needed to explicitly solvate the newly formed hydronium ion. They also tried with only three water molecules, and the barrier is slightly higher. Following the previous calculations, we added four water molecules into **6** to form complex **7**, from which one water molecule performs a nucleophilic attack on the oxo group. During the O–O bond formation, a proton is transferred to the nearby water molecule. The optimized transition state in the triplet state $^3TS_{OO}$ is shown in Figure 1. The triplet barrier is calculated to be 12.9 kcal/mol relative to **7**, whereas the quintet barrier is 10.3 kcal/mol higher than the triplet one. This step is calculated to be almost isoergonic, and the resulting intermediate **8** is only 0.5 kcal/mol higher than **7**. At $^3TS_{OO}$, the critical O–O bond is 1.73 Å, and the Fe–O bond is elongated to 1.70 Å (1.58 Å in **7**). It should be pointed out that the conformation of $^3TS_{OO}$ is different from the previously reported one. Owing to the presence of a hydrogen bond between a water molecule and the fluoro group (hydrogen bonding distance 1.93 Å), the new transition state is 1.5 kcal/mol lower in energy than the previous one. During the O–O bond formation, one electron with β spin is transferred from a water molecule to the ligand radical cation,

Table 1. Redox potentials [V] of various redox reactions at the B3LYP*-2D and M06L levels.

	Redox Couple	Redox potential [V] B3LYP*-2D	M06L[a]	M06L[b]
I	Fe^{4+}–OH_2 (**2**) + e^- → Fe^{3+}–OH_2 (**1**)	1.07	1.02	–
II	Fe^{4+}–OH (**3**) + (e^-, H^+) → Fe^{3+}–OH_2 (**1**)	1.46	1.16	1.04
III	Fe^{5+}–OH (**4**) + e^- → Fe^{4+}–OH (**3**)	1.36	1.44	1.02
IV	TAML·–Fe^{4+}–OH (**4**) + (e^-, H^+) → Fe^{4+}–OH_2 (**2**)	1.75	1.58	–
V	Fe^{5+}=O (**5**) + (e^-, H^+) → Fe^{4+}–OH (**3**)	1.68	1.49	1.33
VI	TAML·–Fe^{5+}=O (**6**) + e^- → Fe^{5+}=O (**5**)	1.43	1.65	1.09
VII	TAML·–Fe^{5+}=O (**6**) + (e^-, H^+) → TAML·–Fe^{4+}–OH (**4**)	1.75	1.70	1.39
VIII	TAML·–Fe^{4+}-OOH (**10**) + e^- → Fe^{4}-OOH (**9**)	1.29	1.46	–
Mean absolute deviation (MAD)		0.14		–

[a] Present calculations with fitting. [b] Previous calculations.[24]

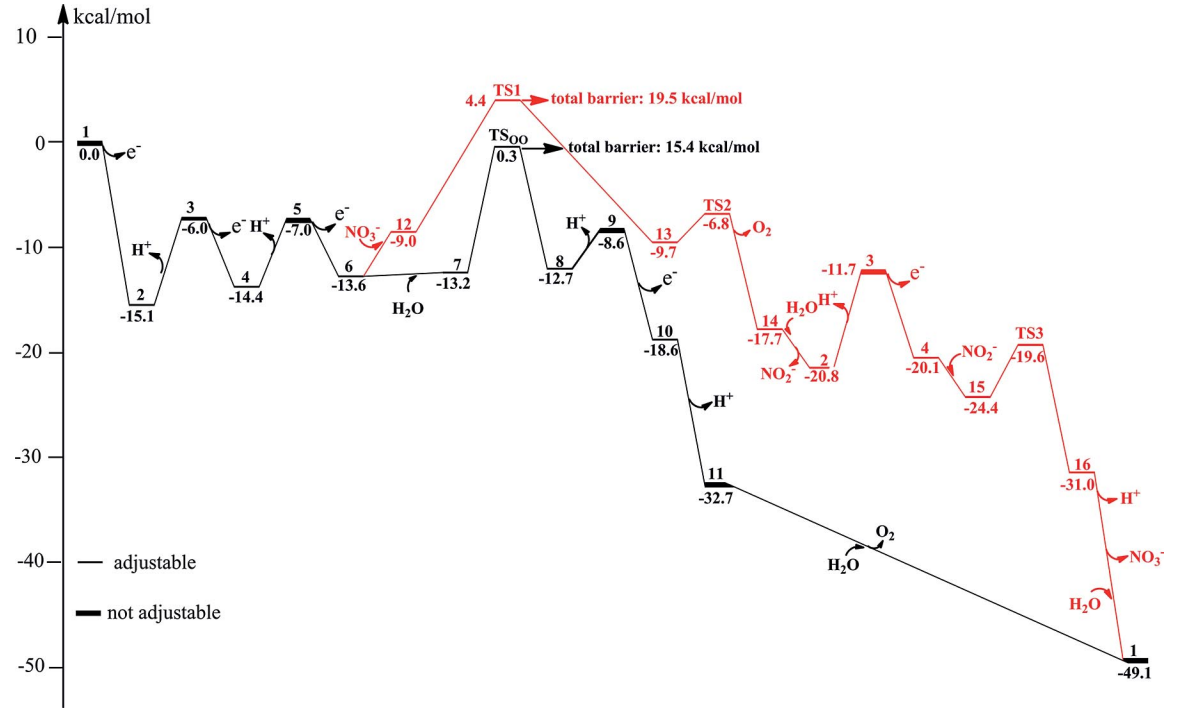

Figure 2. Energy diagram (in kcal/mol at the B3LYP*-2D level) for the two possible catalytic cycles of O_2 formation enabled by WOC_E. The black curve shows O–O bond formation by a water attack, whereas the red curve shows the nitrate attack.

and the other electron with α spin is transferred from the oxo ligand to the metal centre, which leads to the formation of an intermediate-spin Fe^{4+} complex (S_{Fe} = 1). In the following step, a PCET oxidation takes place with the formation of TAML·–Fe^{4+}–OOH (**10**), which is a doublet with the quartet and sextet 5.5 and 7.2 kcal/mol higher in energy, respectively. Further deprotonation of **10** leads to Fe^{3+}–OO (**11**), in which an intermediate-spin iron centre (S_{Fe} = 3/2) is antiferromagnetically coupled to the triplet oxygen molecule (S_{O2} = 1). Partial electron transfer can be seen from the iron atom to the O_2 molecule. The liberation of O_2 and coordination of H_2O can regenerate **1** and start the next catalytic cycle.

From Figure 2, we can see that the oxidative formation of **6** from **2** is endothermic by 1.5 kcal/mol. The O–O bond formation step is rate-limiting and has a total barrier of 15.4 kcal/mol ($^3TS_{OO}$ relative to **2**). The experimental turnover frequency is larger than 1.3 s^{-1} at room temperature and can be converted to a barrier of ca. 17 kcal/mol by using transition-state theory. The calculated barrier is slightly underestimated compared to the experimental one.[21] It should be pointed out that previous CASPT2 calculations showed that the singlet–triplet gap is 3.3 kcal/mol in favour of the singlet state.[24] The present B3LYP*-2D calculations suggest that the triplet is the ground state. If the CASPT2 correction is taken into account, the total barrier becomes 17.2 kcal/mol, which is in excellent agreement with the experimental kinetic results.

In our previous studies on other systems, in which only water binding and O_2 release are involved in the catalytic cycle, the entropy effect was not considered explicitly and two empirical values were adopted, 14 kcal/mol for water binding and 12 kcal/mol for the entropy effects of releasing O_2 gas.[32–38] Here, we also construct the energy diagram (Figure 3) by using this methodology for the formation of an O–O bond by water attack. The process for the binding of water molecules in the second sphere of the complex is set to be thermoneutral, which is quite a good approximation as water is the solvent. The free energy calculations also suggest that this process is endothermic by less than 1 kcal/mol (see Figure 2). For the binding of a water molecule to the metal centre, as in the final ligand exchange step from **11** to **1**, the empirical 14 kcal/mol is used. In Figure 3, the black curve shows the B3LYP*-2D energies including zero-point energy (ZPE) corrections. Two sets of energies are reported. The first set uses the experimental driving force (49.1 kcal/mol) to fit the PCET steps. The second set, shown in parentheses, uses the experimental proton solvation free energy of 264.0 kcal/mol[39] to estimate the energy gain or loss of releasing a proton, for example, from **2**

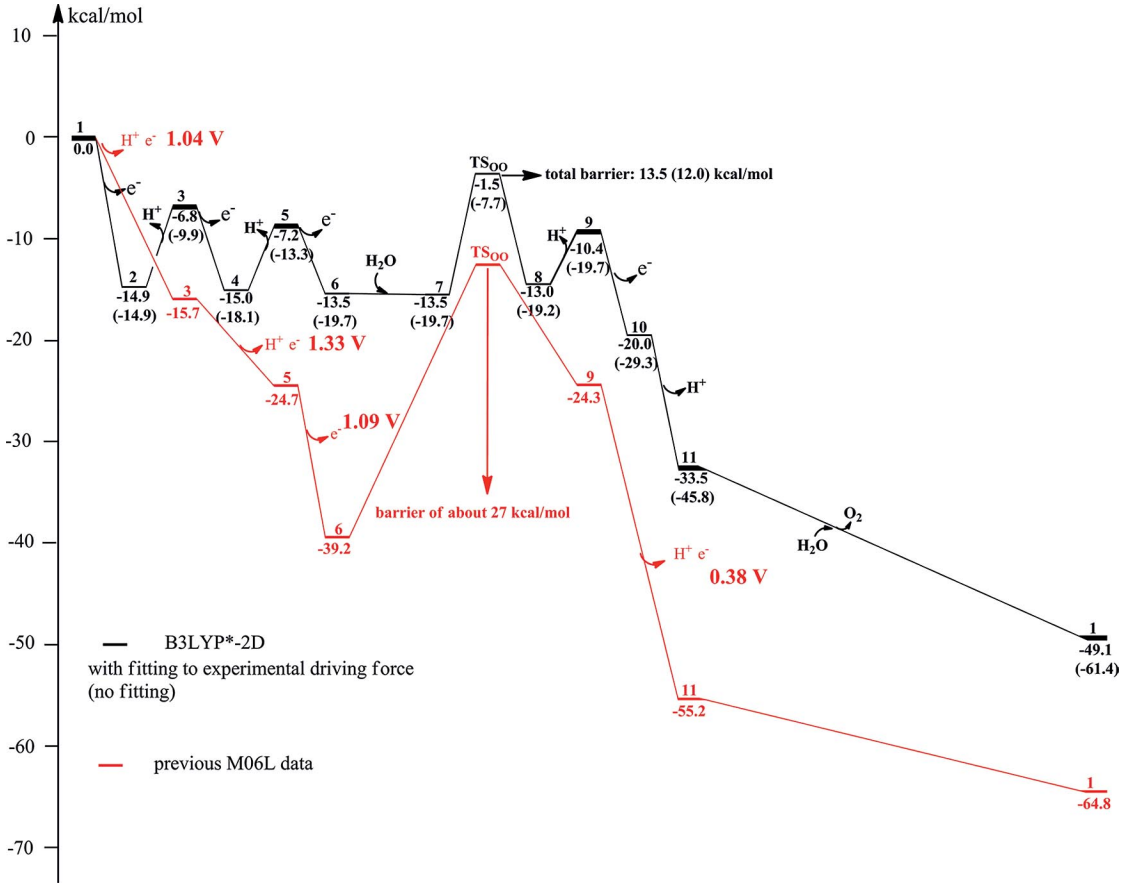

Figure 3. Comparison of energy diagrams of the different methods. The black curve shows the B3LYP*-2D energies with ZPE corrections and an empirical water binding energy of 14 kcal/mol. The red curve shows the previous M06L energies[24] including the relative energies of **9** to **6** and **1** to **11** from the present calculations.

to **3**. The difference between the calculated and the experimental driving force then becomes 12.3 kcal/mol. In addition, the total barrier changes from 13.5 kcal/mol with fitting to 12.0 kcal/mol without fitting. The difference originates from the extra energy cost to reach oxidant **6**. The comparison of the energy diagrams of the four different methodologies, namely, Gibbs free energies with and without fitting the experimental driving force and ZPE-corrected energies with and without fitting the experimental driving force, are shown in Figures S1–S4. The energy diagrams look quite similar, but the total barriers could differ by several kcal/mol depending on the energy penalty for the formation of **6**.

An energy diagram (Figure 3, red curve) is also constructed by using the previously calculated redox potential for **1** to **3**, **3** to **5**, **5** to **6** and **9** to **11** at the M06L level. As the previous study did not report the relative energies of **9** to **6** and **1** to **11** (exchange of O_2 by water), the relative energies from the present M06L calculations were used. The driving force is estimated to be 64.8 kcal/mol, which is overestimated by ca. 15 kcal/mol compared to the experimental value. The M06L energies from our calculations were also used to construct energy diagrams for comparison (Figures S5 and S6). In the previous study, the redox potentials of the four reported couples (**1/3**, **3/5**, **5/6** and **9/11**, Table 1) were calculated to be 1.04, 1.33, 1.09 and 0.38 V, respectively. Our calculations with the M06L functional give 1.00, 1.32, 1.29 and 0.44 V, respectively. The large discrepancy for the **5/6** couple is caused by the CASPT2 corrections used for the singlet–triplet gap of **6** in the previous study, in which the triplet is 3.3 kcal/mol higher in energy than the singlet at the CASPT2 level.[24]

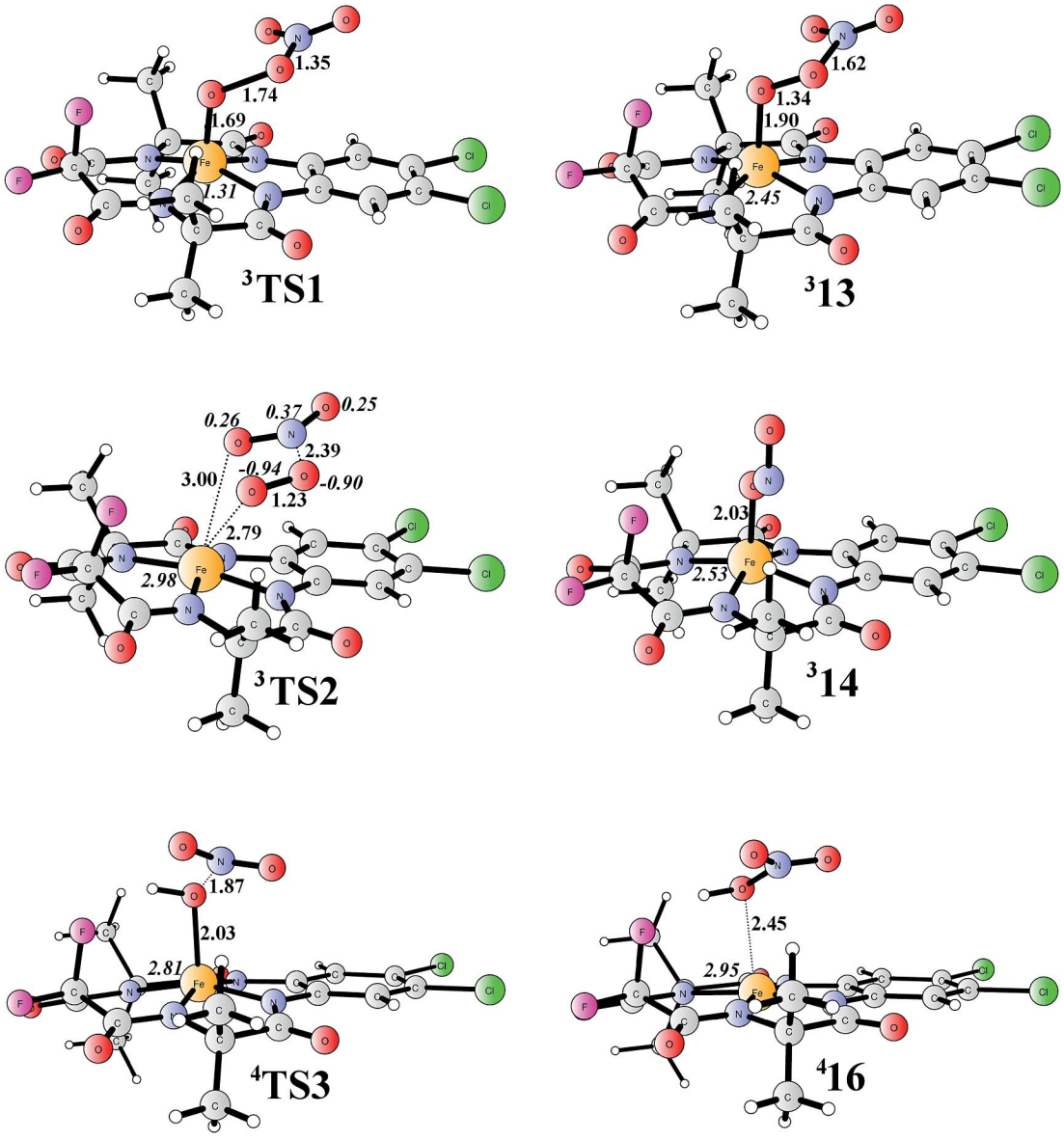

Figure 4. Selected optimized structures along the reaction pathway of nitrate attack.

B. O_2 Formation by Nitrate Attack

An alternative O–O bond formation pathway has been considered here, in which a nitrate ion performs the nucleophilic attack on the oxo group of **6**. The involvement of nitrate ions in water oxidation has been proposed in Ru-based catalysts,[40,41] but has not yet been confirmed by theoretical calculations. As excess ceric ammonium nitrate is used as the oxidant, free nitrate ions could be available and could function as a nucleophile. The interaction of a nitrate ion and **6** to form **12** is endergonic by 4.6 kcal/mol, mainly because of the entropy lost. The optimized transition state of the nitrate attack in the triplet state (^{3}TS1) is shown in Figure 4. The barrier is calculated to be 18.0 kcal/mol relative to the isolated reactants (**6** and a nitrate ion). The quintet barrier is 9.4 kcal/mol higher than the triplet and is similar to that in the water attack. The attack leads to the formation of a peroxynitrate intermediate bound to the ferryl ion (**13**), which lies at –0.7 kcal/mol relative to **12**. From **13**, N–O bond cleavage via TS2 leads to the formation of O_2, which is concomitant with O_2 release and the nitrite ion binding to the metal. This step is associated with a very small barrier of 2.9 kcal/mol relative to **13** in the triplet state.

During the reaction, an oxygen atom is transferred from the nitrate ion to the oxo group, coupled with two-electron reduction to form a ferryl nitrite complex. The newly formed nitrite complex can be oxidized to regenerate a nitrate ion. The exchange of the nitrite ligand in **14** by a water molecule leads to the formation of **2**, which can then be oxidized to **4**. Complex **4** is able to oxidize the nitrite ion to form nitric acid, and the corresponding transition state TS3 is shown in Figure 4. This step is calculated to have a barrier of only 4.8 kcal/mol. Further ligand exchange of nitric acid by a water molecule regenerates **1**.

In this mechanism, the nitrate ion acts as a cocatalyst for the formation of O_2, in which one oxygen atom in the oxygen molecule originates from a nitrate ion. The total barrier is calculated to be 19.5 kcal/mol, which is 4.1 kcal/mol higher than that for the water attack pathway. Isotope labelling by using H_2O^{18} would be helpful to verify whether nitrate is involved in the catalysis. It should be pointed out that nitric acid may oxidize **1** to form **2** and nitrogen dioxide [Equation (1)]. Calculations show that Equation 1 is endothermic by 3.5 kcal/mol. This reaction and its reverse reaction could lead to oxygen exchange between nitric acid and water. The isotope labelling with H_2O^{18} will only work if this exchange process is much slower than water oxidation. Another possible strategy is to measure the kinetic isotope effect of N^{15}/N^{14} by labelling the nitrate nitrogen atoms.

$$\begin{array}{l} \text{TMAL-Fe}^{3+}\text{-OH}_2\ (\mathbf{1}) \quad + \text{NO}_3^- + 2\text{H}^+ \\ \qquad\qquad\qquad\qquad \downarrow \\ \text{TMAL-Fe}^{4+}\text{-OH}_2\ (\mathbf{2}) \quad + \text{H}_2\text{O} \ + \text{NO}_2 \end{array} \qquad (1)$$

C. Competing Pathways

A number of conceivable competing pathways have been studied to understand the experimentally observed degradation of the catalyst, which was not considered in the previous computational study.[24] The potential energy profiles are shown in Figure 5, and selected optimized structures are shown in Figures 6 and 7.

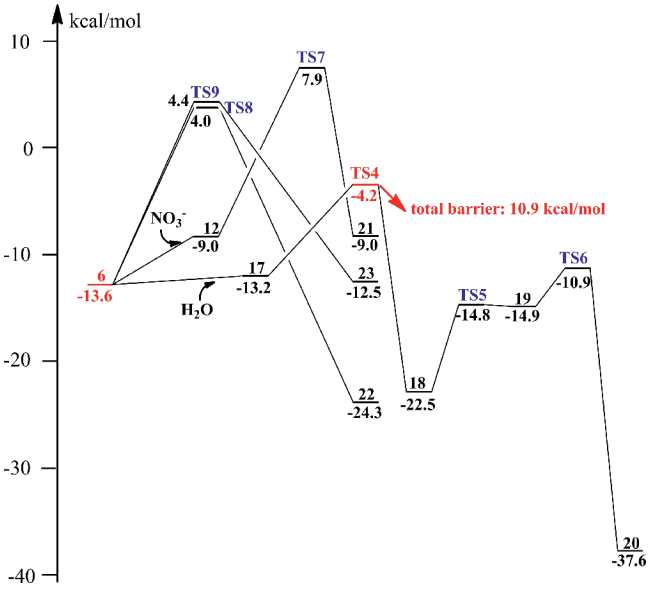

Figure 5. Energy diagram (in kcal/mol at the B3LYP*-2D level) for competing pathways.

As discussed above, water functions as a nucleophile to attack the oxo group and leads to O–O bond formation and reduction of the metal centre and ligand radical cation. An alternative target for the attack would be the ligand radical cation, which has been proposed for the blue dimer.[42,43] Therefore, one water molecule was added to **6** to form **17**. We found that the oxo group acts as a general base and removes a proton from the water molecule, concomitant with a nucleophilic attack on one of the benzene carbon atoms by the emerging hydroxide ion. No proton is released into solution, and, therefore, no additional water molecules are needed to explicitly solvate the system. The use of the continuum solvation model should be capable of describing the solvation effect. The attack proceeds in the triplet state and is associated with a barrier of only 10.9 kcal/mol relative to **2**, which is 4.5 kcal/mol lower than the desired O_2 formation pathway. This could be the origin of the observed catalyst degradation. The attack by the quintet is energetically not feasible (25.1 kcal/mol relative to **2**), and the barrier is, thus, ca. 14 kcal/mol higher than the triplet one. This step was found to be exergonic by 9.7 kcal/mol (**18** relative to **17**), in contrast to the attack on the oxo group, which is close to isoergonic (+0.5 kcal/mol). In the subsequent step, the ferryl-bound hydroxide ion abstracts a proton from the alcohol to form alkoxide intermediate **19**. Finally, the oxyanion performs a nucleophilic attack on one of the benzene carbon atoms, which may lead to the formation of an epoxide via TS6. However, geometry relaxation results in the

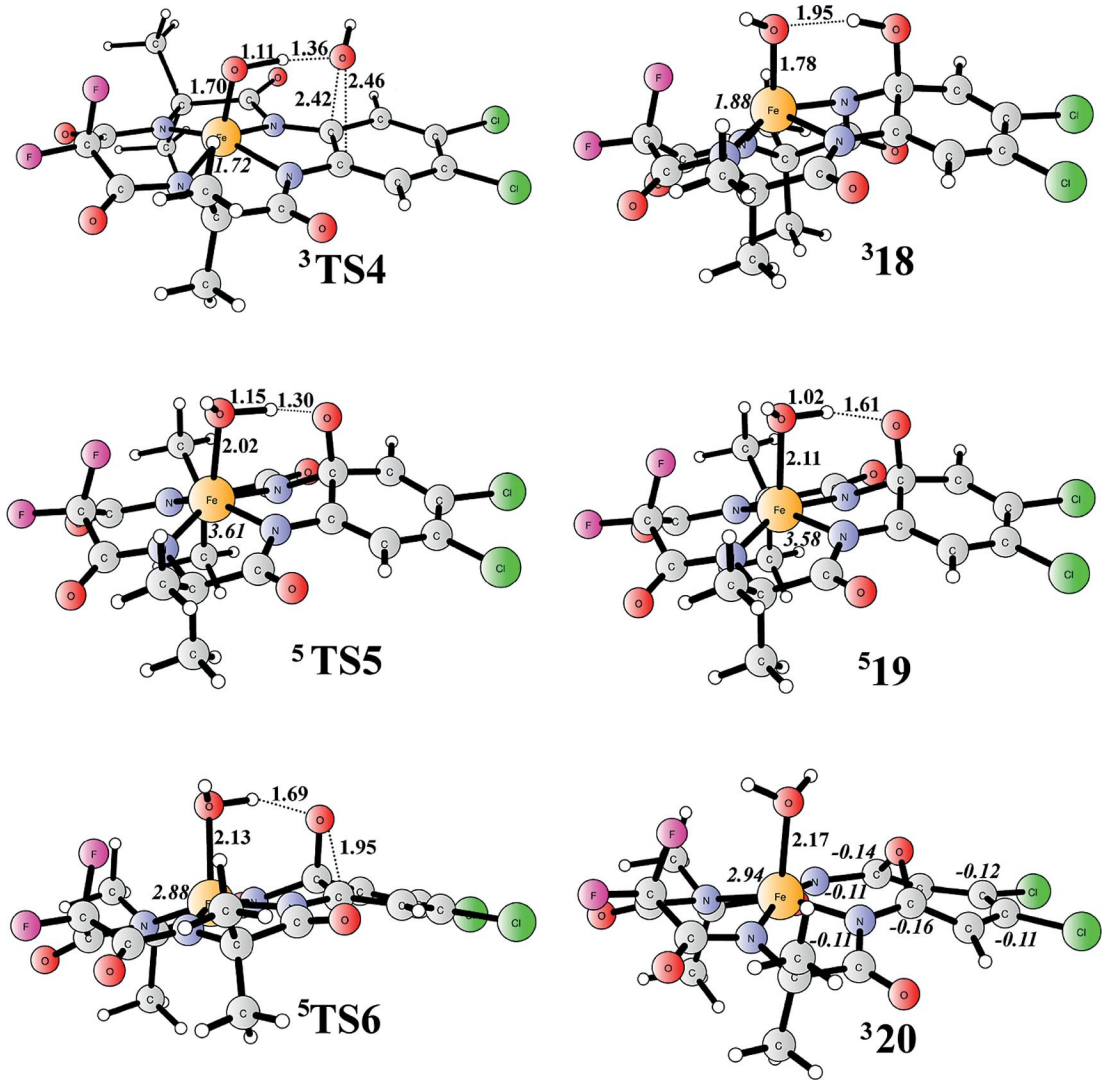

Figure 6. Selected optimized structures along the reaction pathway of ligand degradation by water attack.

epoxide C–C bond cleavage with the formation of a seven-membered ring product, complex **20**, which is similar to those found in extradiol dioxygenase,[44] intradiol dioxygenase[45] and homogentisate dioxygenase.[46] The barrier for such oxygen insertion (^{5}TS6) in the quintet state is very feasible (11.6 kcal/mol relative to **18**). This side-reaction is exergonic by as much as 24.0 kcal/mol (from **6** to **20**), which suggests that the catalyst degradation by this pathway would be irreversible.

The second possible pathway for ligand modification is that a nitrate ion could also perform a nucleophilic attack on the ligand benzene ring. The transition state for the attack at the CH carbon atom in the triplet state (^{3}TS7) is shown in Figure 7, and the barrier is calculated to be 21.5 kcal/mol relative to **6**. Thus, when a nitrate ion participates in the reaction, it prefers to attack the oxo group by 3.5 kcal/mol rather than the ligand. This is different from water, which prefers to attack the ligand, rather than the oxo group.

Another possibility is the self-oxidation of the ligand amide by the Fe^{5+}=O group to form an N-oxide by reductive elimination. The attack can be either on the amide group that is close to the CF_2 group (TS8, Figure 7) or on the amide group that is connected to the benzene ring (TS9, Figure 7). The former one has a barrier of 17.6 kcal/mol relative to **6**, and the reaction is exothermic by 10.7 kcal/mol. The latter one has a slightly higher barrier (18.0 kcal/mol), and the reaction is close to thermoneutral.

The calculations show that the water attack on the ligand is the main catalyst degradation pathway, and **20** is the major product. Thus, the performance of the catalyst depends on the relative barriers of the water attack on the oxo group and on the ligand. As O_2 formation can be observed for ca. 15 cycles, the relative barrier for the ligand modification seems to be underestimated somewhat when using both the B3LYP*-2D and the M06L functionals.

It is also important to check whether **20** has water oxidation activity. If similar barriers are observed, the modified catalyst could also contribute to the TON. The electronic structure of **20** can be described as an intermediate-spin ferric ion antiferromagnetically coupled with a ligand radical. Two sequential PCET oxidations of **20** lead to the

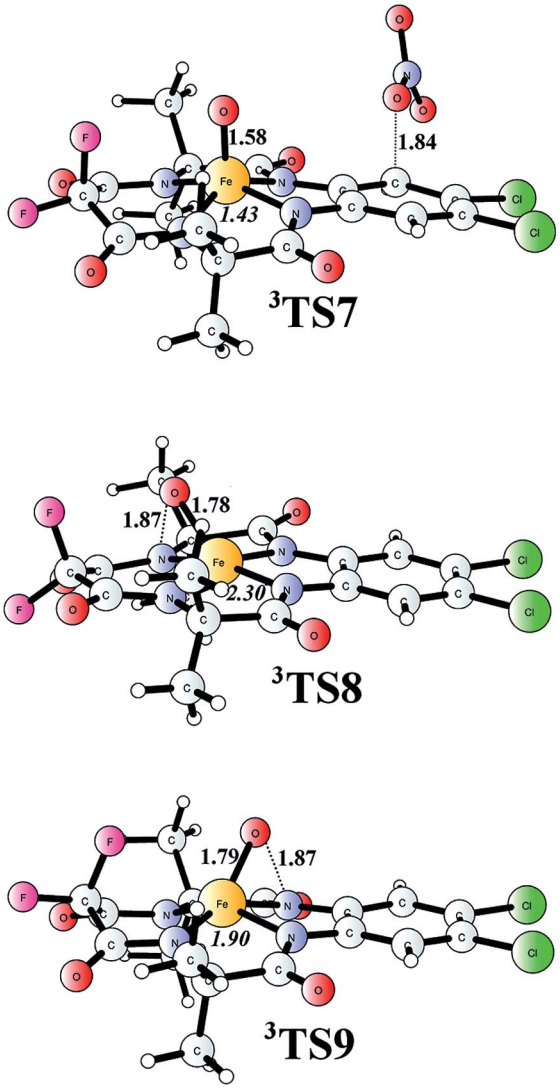

Figure 7. Selected optimized structures along the reaction pathway of ligand degradation by nitrate attack and self-oxidation.

formation of **27** (Figure 8), which is characterized as a ferryl–oxo species. During the oxidation, one electron is removed from the ligand, and the other one is removed from the metal centre. This explains the quite different redox potentials between the modified and unmodified catalyst, for example, the redox potential of the $TAML^{3-}$·Fe^{4+}=O/$TAML^{2-}Fe^{4+}$=O (**26** to **27**) couple is 0.92 V. In **24**, **25** and **27**, the ligand is in the diimine form and has a total charge of –2, rather than –3 as in **6**, **20** and **26**.

From **27**, water continues to perform a nucleophilic attack on the ligand seven-membered ring (TS10) to form an alcohol intermediate **29**. During the attack, a proton is transferred to the oxo group. The barrier for this step is calculated to be only 5.0 kcal/mol (Figure 9) in the triplet state, which is even lower than that for the initial water attack (TS4). In the following step, the metal-bound hydroxide ion abstracts a proton from the alcohol intermediate, coupled with the opening of the seven-membered ring. This step is also associated with a very low barrier of 3.7 kcal/mol in the quintet state. The reaction is exothermic by more than 50 kcal/mol (from **28** to **30**).

We also tried water oxidation from **27**. However, owing to the relatively low oxidation state (Fe^{4+}=O) of **27**, much higher barriers of 26.0 and 27.8 kcal/mol are obtained for both the water attack and the nitrate attack, respectively. These results suggest that when the ligand is modified, water oxidation to form O_2 becomes even more difficult. To increase the TON of the catalyst, one needs to modify or design a more stable ligand to prevent the destructive water attack.

It should be pointed out that further oxidation of **30** is rather difficult. Our calculations show that oxidation of **30** to form an Fe^{5+}=O species by removing two protons and one electron is endothermic by 11.1 kcal/mol (Figure S10), which corresponds to a redox potential of ca. 2.2 V. The main reason for the high redox potential is that the π conjugation of the ligand is broken, which makes the oxidation of the ligand difficult.

Of course, we cannot rule out other possible changes from **30** that could recover some water oxidation activity. An extensive investigation on this issue is beyond the scope of the present study.

D. O_2 Formation by Other Ligands

To rationalize the lack of activity of WOC_A and the relatively lower activity of other catalysts, we optimized all relevant intermediate and transition-state structures and constructed the corresponding energy diagrams, which are displayed in Figures 10–13. A summary of the total barriers is shown in Table 2.

Table 2. Summary of total barriers (in kcal/mol at the B3LYP*-2D level) for various pathways for all five catalysts.

	Total barrier for O_2 formation		Total barrier for ligand oxidation	
	Water attack	Nitrate attack	Water attack	C–H activation
WOC_A	19.7	23.4	9.8	12.5
WOC_B	20.9	25.0	8.7	–
WOC_C	16.3	18.7	9.3	–
WOC_D	15.8	17.2	14.0	–
WOC_E	15.4	19.5	10.9	–

In WOC_A and WOC_B, R^1 is electron-donating, which results in lower redox potentials compared to that of WOC_E. This can be confirmed from the larger exergonicity during the complex oxidation. In WOC_E, the generation of **6** from **2** is slightly endergonic by 1.5 kcal/mol. In WOC_A and WOC_B, it is exergonic by 1.5 and 3.9 kcal/mol, respectively. In WOC_C and WOC_D, R^1 is electron-withdrawing, and their redox potentials are higher than those for WOC_A and WOC_B. WOC_D has a nitro group attached to its benzene ring and, thus, has the highest redox potential. Consequently, the generation of **6** is endergonic by 2.6 kcal/mol, which will contribute to the total barrier for this catalyst.

In WOC_A, R^1 is a methyl group, which can undergo C–H activation to generate an alcohol. The transition state

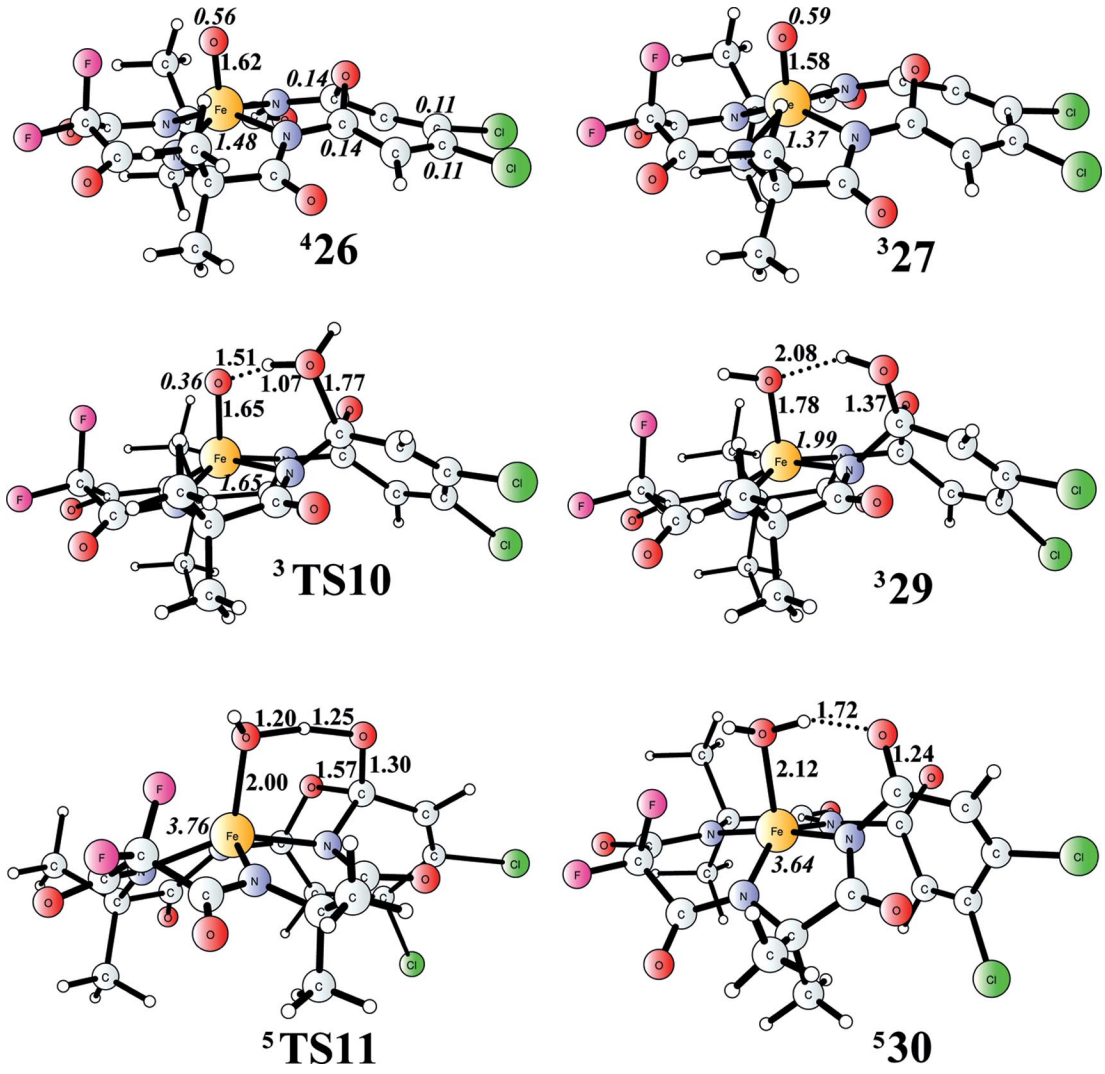

Figure 8. Selected optimized structures along the reaction pathway of ligand degradation by the second water attack.

is shown in Figure 14, and the calculated energy barrier is 12.5 kcal/mol relative to $\mathbf{6}_A$. In addition, the barrier for O_2 formation by water attack is 19.7 kcal/mol. This is 4.3 kcal/mol higher than that of WOC_E, and the difference is very similar to that found in the previous calculations.[24] These two factors could explain why only a small activity can be observed for WOC_A. The C–H activation side-reaction can be avoided by introducing –F or $–CH_2$ substituents, as shown in WOC_B to WOC_E.

In WOC_B, both pathways that lead to O_2 formation have significantly higher barriers than those for WOC_E, whereas the barrier for the water attack on the ligand is 2.2 kcal/mol lower than that that for WOC_E. WOC_C and WOC_D have slightly higher barriers for the water attack on the oxo group, but somewhat lower barriers for the nitrate attack on the oxo group. As the water attack will be the dominant pathway for O_2 formation for all of them, the calculations reproduce quite well the trends for the relative reactivities of these catalysts.

The electronic properties of the ligand are crucial for the catalyst efficiency. Electron-donating substituents favour the thermodynamics of the oxidation but disfavour the reductive O–O bond formation. In contrast, electron-withdrawing substituents make the oxidation thermodynamically less favourable but facilitate the subsequent O–O bond formation. Therefore, the substituents need to be well-balanced to achieve the highest turnover frequency.

E. Comparison of B3LYP*-2D and M06L

The calculated redox potentials of various couples in WOC_E at the B3LYP*-2D and M06L levels are listed in Table 1. The mean absolute deviation is 0.17 V, and the largest deviation is 0.36 V for the PCET oxidation of Fe^{3+}–OH_2. In both methods, the highest redox potential is close to that of CAN (1.72 V), which suggests that the generation of oxidant **6** is possible. It should be pointed out

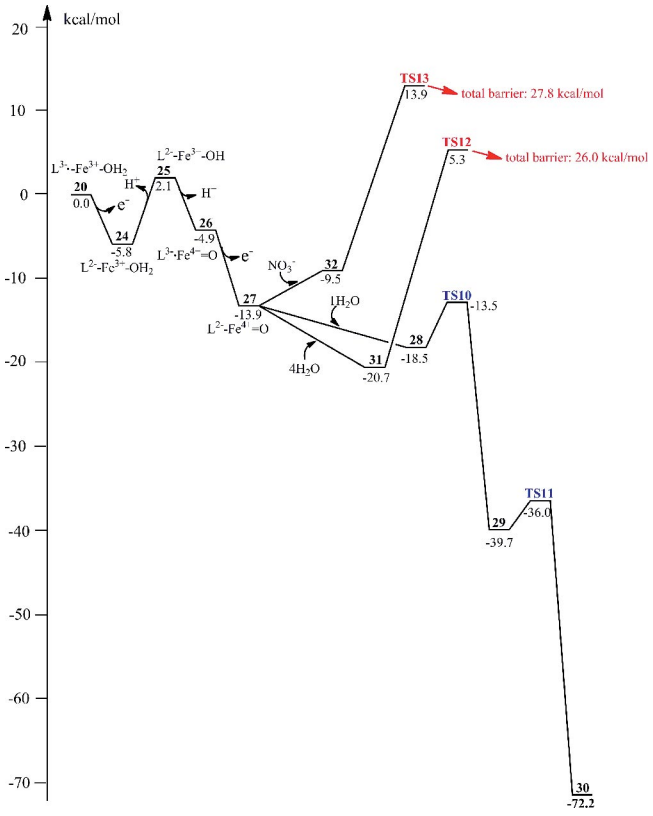

Figure 9. Energy diagram (at the B3LYP*-2D level) for various pathways starting from the modified catalyst **20**. The energy of **20** is set to 0. L is the modified ligand.

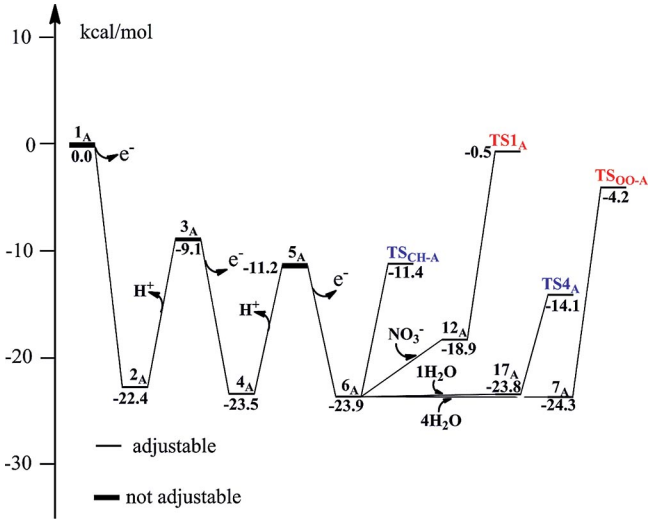

Figure 10. Energy diagram (in kcal/mol at the B3LYP*-2D level) for WOC_A.

that the reference Ce^{4+}/Ce^{3+} couple for M06L is shifted from 138.4 to 130 kcal/mol. Consequently, the reported one-electron redox potential is shifted by +0.36 V.

The energy diagrams at the M06L levels for all five catalysts are summarized in the Supporting Information (Figures S5–S8 and S11–S17), as are the total barriers for various pathways (Table S13).

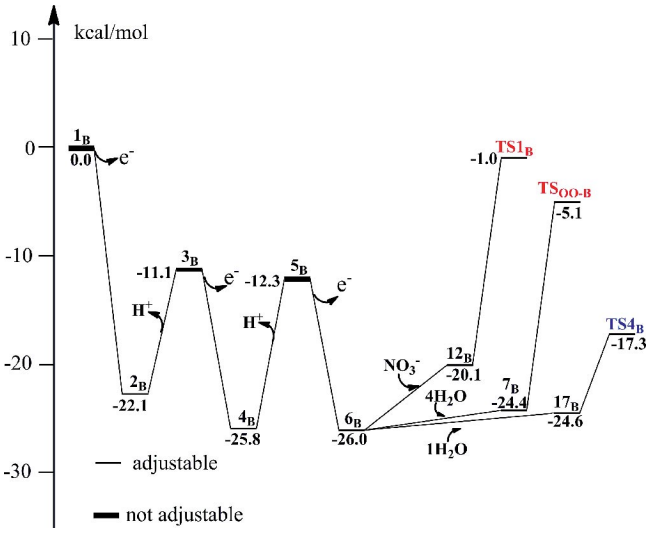

Figure 11. Energy diagram (in kcal/mol at the B3LYP*-2D level) for WOC_B.

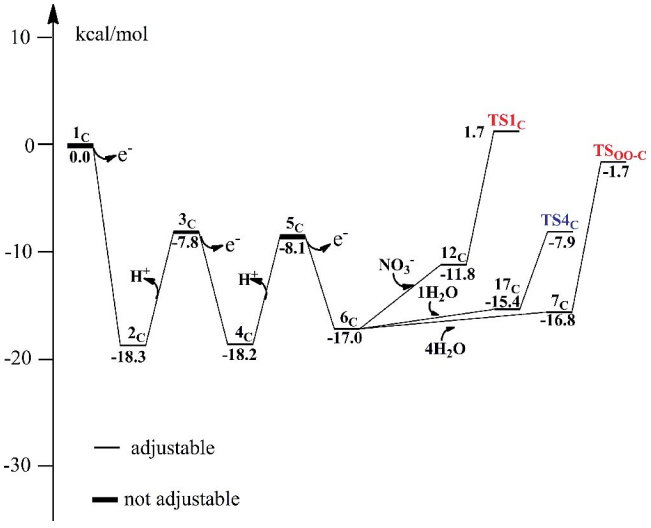

Figure 12. Energy diagram (in kcal/mol at the B3LYP*-2D level) for WOC_C.

For all catalysts, the nitrate attack becomes the preferred pathway in the O_2 formation at the M06L level. For example, the barrier for the water attack on the oxo group is calculated to be 26.0 kcal/mol in the triplet state, which is very close to the barrier reported previously (about 30 kcal/mol) when the singlet–triplet gap at the CASPT2 level (3.3 kcal/mol) is included. Instead, the nitrate attack on the oxo group has a barrier of 19.7 kcal/mol, which is ca. 6 kcal/mol lower than that for the water attack. Thus, these two functionals predict different favoured pathways for the O_2 formation. However, as the catalyst degradation by water attack on the ligand also has a lower barrier (16.6 kcal/mol) at the M06L level, both functionals suggest that the ligand modification proceeds faster than the desired O_2 formation.

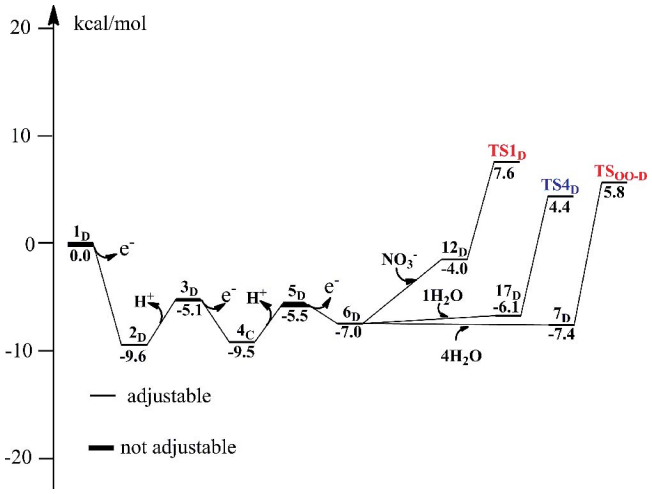

Figure 13. Energy diagram (in kcal/mol at the B3LYP*-2D level) for WOC_D.

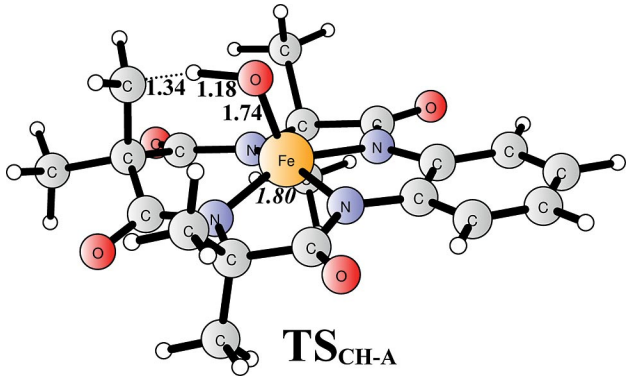

Figure 14. Optimized ligand C–H activation transition state for WOC_A.

Conclusions

In the present study, we have investigated the reaction mechanism of water oxidation catalyzed by iron–TAML complexes by using DFT calculations. Several possible reaction pathways were considered and full energy diagrams were constructed.

Two feasible pathways on the basis of a single metal site have been found for the O_2 formation. Catalysis involving the formation of a dimer, which has been proposed for potassium ferrate[47] and Ru-based catalysts,[11,22] was not considered as the water oxidation by this catalyst is first order. The key oxidant is TAML·–Fe^{5+}=O, which in agreement with the previous study,[24] is formed from TAML–Fe^{3+}–OH_2 by the removal of three electrons and two protons.

In the following step, a water molecule or a nitrate ion can perform a nucleophilic attack on the metal–oxo group, which leads to O–O bond formation. The water attack, here modelled by adding three additional water molecules, leads to the formation of a ferryl peroxide intermediate. This step is calculated to be rate-limiting and has a total barrier of 15.4 kcal/mol in the triplet state. Further oxidation by removing two protons and one electron gives a TAML–Fe^{3+}–O_2 complex, which undergoes ligand exchange with water to regenerate the starting TAML–Fe^{3+}–OH_2 complex. The alternative nitrate attack results in the formation of a ferryl peroxynitrate intermediate, from which N–O bond cleavage occurs and is coupled with O_2 release and binding of the nitrite ion to the metal centre. The attack is calculated to be rate-limiting with a barrier of 19.5 kcal/mol in the triplet state, which is only 4.1 kcal/mol higher than that for water attack. From the ferryl nitrite complex, ligand exchange with water occurs, followed by oxidation to TAML·–Fe^{4+}–OH, which can oxidize the nitrite ion to regenerate a nitrate ion. In this mechanism, the nitrate ion functions as a cocatalyst for O_2 formation, in a process in which one of the oxygen atoms in the generated O_2 molecule originates from a nitrate ion. Further isotope labelling of water and nitrate would be helpful to confirm whether nitrate ions are involved in the catalysis.

Three possible ligand modification pathways have been located to understand the low stability of this catalyst. The calculations demonstrate that water can perform nucleophilic attack on the ligand in a process that is associated with an even lower barrier (only 10.9 kcal/mol) than those for the desired O_2 formation pathways. The oxidative formation of a ligand radical opens the possibility for ligand modification and, thus, might become a drawback of the catalyst. Future ligand design for water oxidation should try to prevent this side-reaction. Further oxidation of the modified ligand leads to the second water attack, which results in the ring-opening and deactivation of the catalyst owing to the rather high redox potential for the following oxidation. Two additional pathways involving a nitrate attack on the ligand and a self-oxidation by reductive elimination to form an N-oxide have higher barriers. The ligand oxidation in this mononuclear iron catalyst should be one of the bottlenecks for electrochemical water oxidation in industrial applications. In addition, ligand oxidation should also be concerned for other homogeneous transition-metal-based catalysts[8–16] in future studies.

An examination of the WOC_A catalyst shows that the two O_2 formation pathways have higher barriers than those of WOC_E, whereas the water attack on the ligand is even lower in energy. In addition, C–H activation of the methyl substituent to form an alcohol is another possible ligand modification pathway. These two competing pathways may explain why only a small activity has been observed for WOC_A. For other catalysts, we find that the barrier for the O_2 formation by water attack decreases from a ligand with more electron-donating substituents to a ligand with more electron-withdrawing substituents. However, the oxidation becomes more difficult and an extra energetic penalty needs to be added to the total barrier. Therefore, a ligand must be optimized with a balance of electron-donating and electron-withdrawing substituents.

Computational Details

The geometry optimizations presented here were accomplished with the M06L[48] functional by using the resolution-of-the-identity

(RI) approximation[49] as implemented in the Gaussian09[50] program package. An automatically generated density-fitting basis set[48] was used for all RI-M06L calculations. The SDD[51] pseudopotential was used for Fe, and 6-31+G(d) was used for all other elements. On the basis of these optimized geometries, more accurate energies were obtained by performing single-point calculations with a larger basis set, in which all elements, except Fe, were described by 6-311+G(2df,p) at both the M06L and the B3LYP* functional (15% exact exchange) levels.[52–54] Solvation effects from the water solvent were taken into account by employing the SMD[55] continuum solvation model at both the M06L and the B3LYP* levels, in the former case with the medium basis set and in the latter with the larger basis set. Analytical frequency calculations were performed at the same level of theory as the geometry optimization to obtain the Gibbs free energy corrections and to confirm the nature of the various stationary points. For all species except water, the concentration correction of 1.9 kcal/mol [RTln(24.5)] at room temperature was added, which is derived from the free-energy change of 1 mol of an ideal gas from 1 atm (24.5 L/mol, 298.15 K) to 1 M (1 mol/L). In the case of water, the concentration correction is 4.3 kcal/mol as the standard state of water is 55.6 M. In addition, the experimental solvation free energy of water (–6.3 kcal/mol) was used.[56] Unless otherwise specified, we report the B3LYP* energies including Gibbs free energy corrections from M06L and dispersion corrections proposed by Grimme (B3LYP*-2D).[57] The M06L relative energies are reported in the Supporting Information.

To build the energy diagram for the full catalytic cycle, the total exergonicity derived from experiment was used. In the present case, the redox potential for the O_2/H_2O couple is 1.19 V at the working pH (0.7). The redox potential for the Ce^{4+}/Ce^{3+} couple is 1.72 V and is pH-independent as no proton is involved in the redox reaction. Thus, the whole water oxidation reaction is exothermic by 49.1 kcal/mol. Four electrons and four protons are released during one catalytic cycle of water oxidation. As the species before and after the removal of one electron and one proton at each step have the same total charge, the solvation free energy difference of the redox couple is quite small and can be well-captured by the continuum solvation model. Therefore, the relative redox potentials of the four PCET oxidation steps can be calculated quite accurately. The absolute redox potentials can be derived by a fit to the above experimental driving force (49.1 kcal/mol). The individual redox potential for the releases of only one electron and the pK_a for the removal of one proton are difficult to model with quantitative accuracy because the total charge of the system changes and the solvation from the environment will then play an important role. The absolute redox potential of the Ce^{4+}/Ce^{3+} couple (1.72 + 4.281 V)[58] corresponds to an electron affinity of 138.4 kcal/mol, and this value was used to set up the thermodynamics of such steps from the B3LYP*-2D results. For the M06L results, this value was shifted to 130.0 kcal/mol to adjust the redox potential to the total driving force (49.1 kcal/mol). For WOC_E, the total barrier does not depend on this empirical value and, thus, it will not alter the present conclusion.

Supporting Information (see footnote on the first page of this article): B3LYP*-2D and M06L data, structures and Cartesian coordinates of WOC_E.

Acknowledgments

Computer time was generously provided by the Swedish National Infrastructure for Computing.

[1] S. Romain, L. Vigara, A. Llobet, *Acc. Chem. Res.* **2009**, *42*, 1944–1953.
[2] J. J. Concepcion, J. W. Jurss, M. K. Brennaman, P. G. Hoertz, A. O. T. Patrocinio, N. Y. M. Iha, J. L. Templeton, T. J. Meyer, *Acc. Chem. Res.* **2009**, *42*, 1954–1965.
[3] M. G. Walter, E. L. Warren, J. R. McKone, S. W. Boettcher, Q. Mi, E. A. Santori, N. S. Lewis, *Chem. Rev.* **2010**, *110*, 6446–6473.
[4] B. Limburg, E. Bouwman, S. Bonnet, *Coord. Chem. Rev.* **2012**, *256*, 1451–1467.
[5] D. G. H. Hetterscheid, J. N. H. Reek, *Angew. Chem. Int. Ed.* **2012**, *51*, 9740–9747.
[6] R. Cao, W. Lai, P. Du, *Energy Environ. Sci.* **2012**, *5*, 8134–8157.
[7] D. J. Wasylenko, R. D. Palmer, C. P. Berlinguette, *Chem. Commun.* **2013**, *49*, 218–227.
[8] S. W. Gersten, G. J. Samuels, T. J. Meyer, *J. Am. Chem. Soc.* **1982**, *104*, 4029–4030.
[9] R. Zong, R. Thummel, *J. Am. Chem. Soc.* **2005**, *127*, 12802–12803.
[10] J. J. Concepcion, J. W. Jurss, J. L. Templeton, T. J. Meyer, *J. Am. Chem. Soc.* **2008**, *130*, 16462–16463.
[11] L. Duan, F. Bozoglian, S. Mandal, B. Stewart, T. Privalov, A. Llbet, L. Sun, *Nat. Chem.* **2012**, *4*, 418–423.
[12] M. D. Kärkäs, T. Åkermark, E. V. Johnston, S. R. Karim, T. M. Laine, B.-L. Lee, T. Åkermark, T. Privalov, B. Åkermark, *Angew. Chem. Int. Ed.* **2012**, *51*, 11589–11593.
[13] N. D. McDaniel, F. J. Coughlin, L. L. Tinker, S. Bernhard, *J. Am. Chem. Soc.* **2008**, *130*, 210–217.
[14] J. F. Hull, D. Balcells, J. D. Blakemore, C. D. Incarvito, O. Eisenstein, G. W. Brudvig, R. H. Crabtree, *J. Am. Chem. Soc.* **2009**, *131*, 8730–8731.
[15] A. Savini, G. Bellachioma, G. Ciancaleoni, C. Zuccaccia, D. Zuccaccia, A. Macchioni, *Chem. Commun.* **2010**, *46*, 9218–9219.
[16] D. G. H. Hetterscheid, J. N. H. Reek, *Chem. Commun.* **2011**, *47*, 2712–2714.
[17] D. K. Dogutan, R. McGuire Jr., D. G. Nocera, *J. Am. Chem. Soc.* **2011**, *133*, 9178–9180.
[18] J. L. Fillol, Z. Codolà, I. Garcia-Bosch, L. Gómez, J. J. Pla, M. Costas, *Nat. Chem.* **2011**, *3*, 807–813.
[19] E. A. Karlsson, B.-L. Lee, T. Åkermark, E. V. Johnston, M. D. Kärkäs, J. Sun, Ö. Hansson, J.-E. Bäckvall, B. Åkermark, *Angew. Chem.* **2011**, *123*, 11919; *Angew. Chem. Int. Ed.* **2011**, *50*, 11715–11718.
[20] S. M. Barnett, K. I. Glodberg, J. M. Mayer, *Nat. Chem.* **2012**, *4*, 498–502.
[21] W. C. Ellis, N. D. McDaniel, S. Bernhard, T. J. Collins, *J. Am. Chem. Soc.* **2010**, *132*, 10990–10991.
[22] J. Nyhlén, L. Duan, B. Åkermark, L. Sun, T. Privalov, *Angew. Chem.* **2010**, *122*, 1817; *Angew. Chem. Int. Ed.* **2010**, *49*, 1773–1777.
[23] X. Lin, X. Hu, J. J. Concepcion, Z. Chen, S. Liu, T. J. Meyer, W. Yang, *Proc. Natl. Acad. Sci. USA* **2012**, *109*, 15669–15672.
[24] M. Z. Ertem, L. Gagliardi, C. J. Cramer, *Chem. Sci.* **2012**, *3*, 1293–1299.
[25] L. Vilella, P. Vidossich, D. Balcells, A. Lledós, *Dalton Trans.* **2011**, *40*, 11241–11247.
[26] T. Privalov, B. Åkermark, L. Sun, *Chem. Eur. J.* **2011**, *17*, 8313–8317.
[27] T. F. Hughes, R. A. Friesner, *J. Phys. Chem. B* **2011**, *115*, 9280–9289.
[28] L. Vigara, M. Z. Ertem, N. Planas, F. Bozoglian, N. Leidel, H. Dau, M. Haumann, L. Gagliardi, C. J. Cramer, A. Llobet, *Chem. Sci.* **2012**, *3*, 2576–2586.
[29] M. Z. Ertem, C. J. Cramer, *Dalton Trans.* **2012**, *41*, 12213–12219.

[30] J. L. Vallés-Pardo, M. C. Guijt, M. Iannuzzi, K. S. Joya, H. J. M. de Groot, F. Buda, *ChemPhysChem* **2012**, *13*, 140–146.
[31] W. Lai, R. Cao, G. Dong, S. Shaik, J. Yao, H. Chen, *J. Phys. Chem. Lett.* **2012**, *3*, 2315–2319.
[32] P. E. M. Siegbahn, *Chem. Eur. J.* **2008**, *14*, 8290–8302.
[33] P. E. M. Siegbahn, *Acc. Chem. Res.* **2009**, *42*, 1871–1880.
[34] M. R. A. Blomberg, P. E. M. Siegbahn, *Biochim. Biophys. Acta* **2010**, *1797*, 129–142.
[35] P. E. M. Siegbahn, M. R. A. Blomberg, *Chem. Rev.* **2010**, *110*, 7040–7061.
[36] X. Li, G. Chen, S. Schinzel, P. E. M. Siegbahn, *Dalton Trans.* **2011**, *40*, 11296–11307.
[37] P. E. M. Siegbahn, *J. Photochem. Photobiol. B: Biology* **2011**, *104*, 94–99.
[38] P. E. M. Siegbahn, *Phys. Chem. Chem. Phys.* **2012**, *14*, 4849–4856.
[39] M. D. Tissandier, K. A. Cowen, W. Y. Feng, E. Gundlach, M. H. Cohen, A. D. Earhart, J. V. Coe, T. R. Tuttle Jr., *J. Phys. Chem. A* **1998**, *102*, 7787–7794.
[40] D. J. Wasylenko, C. Ganesamoorthy, M. A. Henderson, B. D. Koivisto, H. D. Osthoff, C. P. Berlinguette, *J. Am. Chem. Soc.* **2010**, *132*, 16094–16106.
[41] D. J. Wasylenko, C. Ganesamoorthy, M. A. Henderson, C. P. Berlinguette, *Inorg. Chem.* **2011**, *50*, 3662–3672.
[42] J. L. Cape, J. K. Hurst, *J. Am. Chem. Soc.* **2008**, *130*, 827–829.
[43] A. Ozkanlar, J. L. Cape, J. K. Hurst, A. E. Clark, *Inorg. Chem.* **2011**, *50*, 8177–8187.
[44] P. E. M. Siegbahn, F. Haeffner, *J. Am. Chem. Soc.* **2004**, *126*, 8919–8932.
[45] T. Borowski, P. E. M. Siegbahn, *J. Am. Chem. Soc.* **2006**, *128*, 12941–12953.
[46] T. Borowski, V. Georgiev, P. E. M. Siegbahn, *J. Am. Chem. Soc.* **2005**, *127*, 17303–17314.
[47] R. Sarma, A. M. Angeles-Boza, D. W. Brinkley, J. P. Roth, *J. Am. Chem. Soc.* **2012**, *134*, 15371–15386.
[48] Y. Zhao, D. G. Truhlar, *J. Chem. Phys.* **2006**, *125*, 194101.
[49] B. I. Dunlap, *THEOCHEM* **2000**, *529*, 37–40.
[50] M. J. Frisch, G. W. Trucks, H. B. Schlegel, G. E. Scuseria, M. A. Robb, J. R. Cheeseman, G. Scalmani, V. Barone, B. Mennucci, G. A. Petersson, H. Nakatsuji, M. Caricato, X. Li, H. P. Hratchian, A. F. Izmaylov, J. Bloino, G. Zheng, J. L. Sonnenberg, M. Hada, M. Ehara, K. Toyota, R. Fukuda, J. Hasegawa, M. Ishida, T. Nakajima, Y. Honda, O. Kitao, H. Nakai, T. Vreven, J. A. Montgomery, Jr., J. E. Peralta, F. Ogliaro, M. Bearpark, J. J. Heyd, E. Brothers, K. N. Kudin, V. N. Staroverov, R. Kobayashi, J. Normand, K. Raghavachari, A. Rendell, J. C. Burant, S. S. Iyengar, J. Tomasi, M. Cossi, N. Rega, J. M. Millam, M. Klene, J. E. Knox, J. B. Cross, V. Bakken, C. Adamo, J. Jaramillo, R. Gomperts, R. E. Stratmann, O. Yazyev, A. J. Austin, R. Cammi, C. Pomelli, J. W. Ochterski, R. L. Martin, K. Morokuma, V. G. Zakrzewski, G. A. Voth, P. Salvador, J. J. Dannenberg, S. Dapprich, A. D. Daniels, Ö. Farkas, J. B. Foresman, J. V. Ortiz, J. Cioslowski, D. J. Fox, *Gaussian 09*, Revision B.01, Gaussian, Inc., Wallingford, CT, **2009**.
[51] M. Dolg, U. Wedig, H. Stoll, H. Preuss, *J. Chem. Phys.* **1987**, *86*, 866–872.
[52] A. D. Becke, *J. Chem. Phys.* **1993**, *98*, 5648–5652.
[53] M. Reiher, O. Salomon, B. A. Hess, *Theor. Chem. Acc.* **2001**, *107*, 48–55.
[54] P. E. M. Siegbahn, *J. Biol. Inorg. Chem.* **2006**, *11*, 695–701.
[55] A. V. Marenich, C. J. Cramer, D. G. Truhlar, *J. Phys. Chem. B* **2009**, *113*, 6378–6396.
[56] D. M. Camaioni, C. A. Schwerdtfeger, *J. Phys. Chem. A* **2005**, *109*, 10795–10797.
[57] S. Grimme, *J. Comput. Chem.* **2006**, *27*, 1787–1799.
[58] A. A. Isse, A. Gennaro, *J. Phys. Chem. B* **2010**, *114*, 7894–7899.
Received: June 5, 2013
Published Online: September 24, 2013

